This is the accepted version of the following article

Karel Královec, Radim Havelek, Eliška Kročová, Lucie Kučírková, Martina Hauschke, Jan Bartáček, Jiří Palarčík, Miloš Sedlák (2019). Silica coated iron oxide nanoparticles-induced cytotoxicity, genotoxicity and its underlying mechanism in human HK-2 renal proximal tubule epithelial cells. *Mutation Research/Genetic Toxicology and Environmental Mutagenesis.* DOI: 10.1016/j.mrgentox.2019.05.015

This accepted version is available from URI https://hdl.handle.net/10195/74989

Publisher's version is available from:
https://www.sciencedirect.com/science/article/pii/S1383571818304285

This version is licenced under a Creative Commons Attribution-NonCommercial-NoDerivatives 4.0.International.

Mutat Res Gen Tox En xxx (xxxx) xxx–xxx

Contents lists available at ScienceDirect

Mutat Res Gen Tox En

journal homepage: www.elsevier.com/locate/gentox

Silica coated iron oxide nanoparticles-induced cytotoxicity, genotoxicity and its underlying mechanism in human HK-2 renal proximal tubule epithelial cells

Karel Královec[a,*], Radim Havelek[b], Eliška Kročová[a], Lucie Kučírková[a], Martina Hauschke[a], Jan Bartáček[c], Jiří Palarčík[d], Miloš Sedlák[c]

[a] Department of Biological and Biochemical Sciences, Faculty of Chemical Technology, University of Pardubice, Studentská 573, Pardubice 532 10, Czech Republic
[b] Department of Medical Biochemistry, Faculty of Medicine in Hradec Králové, Charles University, Šimkova 870, Hradec Králové 500 03, Czech Republic
[c] Institute of Organic Chemistry and Technology, Faculty of Chemical Technology, University of Pardubice, Studentská 573, 532 10 Pardubice, Czech Republic
[d] Institute of Environmental and Chemical Engineering, Faculty of Chemical Technology, University of Pardubice, Studentská 573, 532 10 Pardubice, Czech Republic

ARTICLE INFO

Keywords:
Magnetic nanoparticles
Kidneys
Cytotoxicity
DNA damage
ROS

ABSTRACT

Iron oxide nanoparticles (IONPs) have a great potential with regard to cell labelling, cell tracking, cell separation, magnetic resonance imaging, magnetic hyperthermia, targeted drug and gene delivery. However, a growing body of research has raised concerns about the possible unwanted adverse cytotoxic effects of IONPs. In the present study, the *in vitro* cellular uptake, antiproliferative activity, cytotoxicity, genotoxicity, prooxidant, microtubule-disrupting and apoptosis-inducing effect of Fe_3O_4@SiO_2 and passivated Fe_3O_4@SiO_2-NH_2 nanoparticles on human renal proximal tubule epithelial cells (HK-2) have been studied. Both investigated silica coated IONPs were found to have cell growth-inhibitory activity in a time- and dose-dependent manner. Determination of cell cycle phase distribution by flow cytometry demonstrated a G1 and G2/M phase accumulation of HK-2 cells. A tetrazolium salt cytotoxicity assay at 24 h following treatment demonstrated that cell viability was reduced in a dose-dependent manner. Microscopy observations showed that both Fe_3O_4@SiO_2 and Fe_3O_4@SiO_2-NH_2 nanoparticles accumulated in cells and appeared to have microtubule-disrupting activity. Our study also revealed that short term 1 h exposure to 25 and 100 μg/mL of silica coated IONPs causes genotoxicity. Compared with vehicle control cells, a significantly higher amount of γH2AX foci correlating with an increase in DNA double-strand breaks was observed in Fe_3O_4@SiO_2 and Fe_3O_4@SiO_2-NH_2-treated and immunestained HK-2 cells. The investigated nanoparticles did not trigger significant ROS generation and apoptosis-mediated cell death. In conclusion, these findings provide new insights into the cytotoxicity of silica coated IONPs that may support their further safer use.

1. Introduction

In recent years, there has been an increasing use of iron oxide nanoparticles (IONPs) in a broad range of biomedical applications, including cell labelling and cell tracking [1,2], cell separation [3], magnetic resonance imaging (MRI) [4,5], magnetic hyperthermia [6], targeted drug delivery [7–9] and gene delivery [10]. However, a growing body of research has called into question whether exposure to IONPs may have toxic effects on the surrounding human cells or tissues. Subsequently, these growing safety concerns have been highlighted even more since IONPs have already been used in clinical applications [11].

The kidneys are principally the organs responsible for removing metabolic waste products from the blood, reabsorbing essential nutrients such as glucose and maintaining a water/ion balance in healthy individuals. However, the kidneys are particularly vulnerable to toxic insults caused by a wide range of xenobiotics [12]. No less importantly perhaps, the combination of a high blood supply, large endothelial surface area, high metabolic activity, and unique concentrating ability makes the kidneys potentially vulnerable to damage under the effect of nanoparticles [13–15]. In this regard, Chen et al. [13] observed damage to renal proximal tubular cells in mice exposed to copper nanoparticles. Later, Wang et al. [14] observed the serious pathological change of kidneys in mice following oral administration of titanium dioxide nanoparticles. The other recent animal study by Hanini et al., 2011 revealed that maghemite uncoated γ-Fe_2O_3 nanoparticles can promote

* Corresponding author.
E-mail address: karel.kralovec@upce.cz (K. Královec).

https://doi.org/10.1016/j.mrgentox.2019.05.015
Received 27 November 2018; Received in revised form 20 May 2019; Accepted 29 May 2019
1383-5718/ © 2019 Elsevier B.V. All rights reserved.

cellular damage in the liver, lungs and kidneys of Wistar rats. Histologically observed perivascular inflammation *in vivo* indicated that γ-Fe_2O_3 nanoparticles could damage several organs, such as the lungs and kidneys, through immunological reactions [15].

Although a lot of effort has been devoted to nanotoxicity so far, only a limited number of *in vitro* studies have examined the cytotoxicity of nanoparticles in non-tumour cellular models available for kidney-related research [16–18]. Additionally, no evaluations to-date have specifically focused on the renal cytotoxicity of silica coated Fe_3O_4 IONPs.

The current study is aimed at investigating the *in vitro* antiproliferative, cytotoxic, genotoxic and pro-apoptotic mechanisms of silica coated IONP in human renal proximal tubule epithelial cells (HK-2). Silica is known to be one of the most convenient and widely used coating layer for IONP due to its chemical stability, biocompatibility and ease of functionalization [19–21]. We compared unfunctionalized and functionalized IONPs (Fe_3O_4@SiO_2, Fe_3O_4@SiO_2-NH_2) to evaluate the influence of the coating on the cytotoxicity and genotoxicity. To elucidate the potential mechanisms of renal toxicity of silica coated IONPs, methods measuring various toxicological and cellular endpoints were employed, including XTT tetrazolium salt viability assay, dynamic real-time monitoring of cells proliferation with xCELLigence system, flow cytometry cell cycle analysis, flow cytometry dihydroethidium staining for reactive oxygen species (ROS), microscopy imaging for cellular uptake and accumulation of IONPs, Western blot analysis of expression of proteins involved in-cell death, immunofluorescence labelling for detection of γH2AX, β-tubulin and activated caspase 3/7.

2. Materials and methods

2.1. Preparation and characterization of unfunctionalized Fe_3O_4@SiO_2 IONPs

The starting chemicals and solvents were purchased from Sigma (Sigma–Aldrich, St. Louis, MO, USA) or Fluka (Honeywell, Morris Plains, NJ, USA) and were used without further purification. A round-bottom, three-necked, 500 mL flask equipped with a stirrer and placed in an ultrasonic bath was charged with 80 mg Fe_3O_4 nanoparticles (114 ± 59 nm, DLS) in 20 mL of distilled water [22]. After dispergation for 30 min by the action of ultrasound (450 W), the reaction mixture was treated with a solution of 10 ml of 10% tetrabutylammonium hydroxide and 200 ml of 96% ethanol. Then the stirred (300 rpm) reaction mixture exposed to the constant action of ultrasound was treated with a solution of 140 mg (0.672 mM) tetraethyl orthosilicate in 10 mL of absolute ethanol, added dropwise during 10 min. After stirring for 24 h at 40 °C, the Fe_3O_4@SiO_2 IONPs were separated using a magnet, then washed with distilled water (3 × 50 mL) and methanol (2 × 50 mL) and finally dried in a vacuum lab oven at 40 °C [23]. The yield was 120 mg of Fe_3O_4@SiO_2 IONPs. The specific surface area, FT-IR-spectroscopy and powder X-ray diffraction analysis were identical as we described previously [24].

2.2. Preparation and characterisation of amino-functionalized Fe_3O_4@SiO_2 IONPs

A mixture containing 100 mg of Fe_3O_4@SiO_2, 50 μM of water, 50 mg of α-methoxypoly(ethylene glycol) carboxylic acid (M_w = 5000 g/mole), 10 mg of 4-toluenesulfonic acid and 8 μL of 3-aminopropylethoxysilane in 100 mL of toluene was placed in a round-bottom flask exposed to the action of ultrasound (450 W) for 30 min. The mixture was then refluxed for 62 h. The Fe_3O_4@SiO_2-NH_2 particles were separated using a magnet, washed with methanol (5 × 50 mL) and distilled water (3 × 50 mL), then dried under vacuum at 40 °C [24]. The yield was 100 mg of Fe_3O_4@SiO_2-NH_2 IONPs. The total nitrogen content was determined by microanalysis, and the reactive amino groups content was determined spectrophotometrically [25]. The specific surface area, FT-IR-spectroscopy and powder X-ray diffraction analysis were identical as we described previously [24].

2.3. Dynamic light scattering

Average particle size, polydispersity index (PDI) and zeta potential of the prepared nanoparticles were determined by dynamic lights cattering (DLS) using a Zetasizer Nano ZS (Malvern Panalytical Ltd., Malvern, United Kingdom). The measurements were performed at 25 °C, with a scattering angle of 173°, using disposable sizing cuvettes. The samples were prepared as a suspension of nanoparticles at 1 mg/mL in PBS or at 400 μg/mL in complete cell culture medium. Each measurement was performed in 10 repeats after 30 s. Data were statistically processed.

2.4. General procedures for biological experiments

Fe_3O_4@SiO_2 and Fe_3O_4@SiO_2-NH_2 IONPs: stock solutions of nanoparticles in concentrations of 8 mg/mL were dissolved in PBS (Sigma-Aldrich, St. Louis, MO, USA). Before an experiment, the stock solutions were sonicated for 20 min. to redisperse nanoparticles. For the experiments, the stock solutions were added to the complete cell culture medium containing 5% foetal bovine serum (FBS) to create final concentrations of 1 μg/mL - 400 μg/mL. The negative control was treated with 5% phosphate-buffered saline (PBS). Cells treated with 5% DMSO, cisplatin at 100 μM, doxorubicin at 500 nM and 50 μM, H_2O_2 at 60 μM or nocodazole at 5 μM were used as positive control. Cisplatin, doxorubicin, H_2O_2 and nocodazole were purchased from Sigma-Aldrich (Sigma-Aldrich, St. Louis, MO, USA). To determine antiproliferative activity, we need to follow this after at least first cell doubling, which takes approximately 24 h. For monitoring of DNA double-strand breaks (DSBs), one of the earliest events in the double-stranded DNA break response is the phosphorylation of the histone H2A complement variant, the histone H2AX at serine 139. This resulting local levels of serine 139 phosphorylated H2AX (γH2AX) can be detected by immunofluorescence microscopy, and are termed γH2AX foci. H2AX phosphorylation levels reached a maximum 10 min after introduction DSBs, started to decline between 1 and 2 h, and reached background level 8 to 12 h post DSBs. Therefore, we used 1 -h interval to follow direct DSBs in cells where γH2AX peaks. For each method, three independent cell preparations were evaluated.

2.5. Cell cultures and culture conditions

The experiments were carried out with the HK-2 cell line. HK-2 cells, which are human renal proximal tubular epithelial cells immortalized by transduction with human papilloma virus 16 E6/E7 genes, were obtained from the European Collection of Cell Cultures (ECACC, Salisbury, UK). The HK-2 cells were cultured in a DMEM/F12 (1:1) medium supplemented with 5% FBS, 2 mM L-glutamine, 10 ng/mL epidermal growth factor (EGF), a 10 μg/mL insulin–transferrin–selenium (ITS) solution, 50 μg/mL penicillin and 50 μg/mL streptomycin (all reagents from Life Technologies, Grand Island, NY, USA). The cells were maintained under standard cell culture conditions at 37 °C in a humidified incubator in an atmosphere of 5% CO_2 – 95% air. A CASY Cell Counter and Analyzer (Roche, Basel, Switzerland) were used for basic quality control of the cell culture system and for evaluating cell numbers. HK-2 cells in the maximum range of 20 passages and in an exponential growth phase were used for this study.

2.6. Cell viability

Cell viability was tested using colorimetric XTT II cell proliferation and a viability assay kit (Roche, Basel, Switzerland). Cells were seeded in 96-well plates at a density of 30,000 cells/well. After 24 h, silica coated IONPs were added at various concentrations in triplicates. Cells

ARTICLE IN PRESS

exposed to 5% DMSO were used as a positive control. After a further 24 h, 100 µL of the XTT reagent (2,3-bis-(2-methoxy-4-nitro-5-sulfophenyl)-2H-tetrazolium-5-carboxanilide) was added to each well in a 96-well plate and incubated for 3 h at 37 ˚C. Finally, the absorbance of converted formazan in each well was measured at 470 nm using a Tecan Infinite M200 spectrophotometer (Tecan Group, Männedorf, Switzerland). As a blank ("the zeroing blank") we used cells in media with nanoparticles at time zero – prior the incubation with XTT tetrazolium salt. Viability was calculated as described in the paper by Havelek and colleagues using the following formula: (%) viability = (A470sample - A470blank) / (A470control - A470blank) x 100, where A470 is the absorbance of the utilized XTT formazan measured at 470 nm [26].

2.7. Real-time cellular analysis

The real-time growth kinetics of HK-2 cells was examined using the xCELLigence RTCA (Real-Time Cell Analysis) SP (Single Plate) system (Roche Diagnostic, Mannheim, Germany), allowing label-free, dynamic monitoring of cell adhesion, proliferation and cell death in real-time. Briefly, the xCELLigence system was connected and tested by resistor plate before the RTCA SP station was placed inside the incubator at 37 ˚C and 5% CO_2. Background measurements were taken by adding 100 µL of an appropriate medium to the wells of the E-Plate 96. Cell suspension (90 µL) at a density of 1.7×10^4 of HK-2 cells per well was added to each well of the E-plate 96 and allowed to attach overnight prior to start of treatment. Cell proliferation was dynamically monitored at 30 min. intervals. When the cells entered the logarithmic growth phase, they were treated with 10 µL of dispersed stock solutions of nanoparticles with different concentrations in triplicates to obtain final desired concentrations in each well. Cells treated with 5% DMSO were used as a positive control. After 72 h of incubation with the tested nanoparticles, cell proliferation and the cytotoxic effect were plotted using a characteristic cell index-time profile. Evaluations were performed using RTCA 1.2.1 software (Roche Diagnostic, Mannheim, Germany).

2.8. Genotoxicity γH2AX assay

HK-2 cells were seeded at a density of 300,000 cells/chamber in 2-well glass chamber slides (Thermo Fisher Scientific, Waltham, MA, USA). After 24 h, the spent medium was replaced with a fresh medium and the cells were treated with 25 and 100 µg/mL of silica coated IONPs for 1 h. Cells treated with 50 µM doxorubicin, a topoisomerase II-stabilizing drug that induces DNA double strand breaks, was used as positive control. Subsequently, the cells were fixed with 4% paraformaldehyde, washed (3 × 5 min) with PBS, permeabilized in 0.2% Triton X-100/PBS for 15 min and washed (3 × 5 min) with PBS (reagents from Sigma–Aldrich, St. Louis, MO, USA). Before incubation with primary antibodies (overnight at 4 ˚C), the cells were incubated with 7% inactivated foetal calf serum + 2% bovine serum albumin in PBS for 30 min at room temperature. Rabbit monoclonal anti-phosphohistone H2AX Ser139 (Cell Signaling, Danvers, MA, USA) was used for γH2AX detection. After pre-incubation with a 5.5% donkey serum in PBS for 30 min, the cells were incubated with a secondary antibody for 1 h in the dark at room temperature and washed (3 × 5 min) with PBS. Secondary antibody was affinity purified donkey anti-rabbit-FITC-conjugated, from the Jackson Laboratory (West Grove, PA, USA). The nuclei were counterstained with 4′,6-diamidino-2-phenylindole (DAPI) at 1 µg/mL for 1 h. After three washes in PBS, the slides were mounted with antifading ProLong® Gold mounting medium (Life Technologies, Grand Island, NY, USA). Images of all of the examined slides were obtained by a Nikon epi-fluorescence microscope system Eclipse 80i; the exposure time and dynamic range of the camera in all of the channels were adjusted to the same values for all of the slides to portray quantitatively comparable images. The images were further processed and merged using NIS-Elements Advanced Research 4.13 (instruments and software from Nikon, Tokyo, Japan). Next, each slide was analysed manually for the presence of γH2AX foci and fluorescent foci patterns by visual inspection with the naked eye.

2.9. ROS assay

ROS production in HK-2 cells treated with silica coated IONPs was determined by dihydroethidium (DHE) staining. In cells, DHE reacts with superoxide anion to form 2-dihydroxyethidium (EOH, which exhibits red fluorescence) and ethidium [27]. The HK-2 cells were seeded in 6-well plates (5×10^5 cells per well) and incubated for 24 h at 37 ˚C and in a CO_2 incubator (5%). After seeding (24 h later), the spent medium was replaced with a fresh medium and the cells were treated with 25 and 100 µg/mL of silica coated IONPs, a positive and a negative control, for 1 h at 37 ˚C, in a CO_2 incubator (5%). HK-2 cells treated with 60 µM of H_2O_2 were used as a positive control. After 1 h of exposure, the cells were harvested with 0.05% trypsin and incubated with PBS containing 1 µM of dihydroethidium (DHE) (Sigma–Aldrich, St. Louis, MO, USA) for 30 min in a humidified 37 ˚C, CO_2 incubator (5%) in the dark. Fluorescence was measured using a CyAn flow cytometer (Beckman Coulter, Miami, FL, USA). Excitation and emission wavelengths were 488 and 620 nm respectively. Listmode data were analysed using Summit v4.3 software (Beckman Coulter, Miami, FL, USA).

2.10. Immunofluorescence staining of β-tubulin

These set of experiments were designed to determine whether silica coated IONPs induce morphological changes of the microtubule cytoskeleton. For each condition, 300 000 cells were seeded in 2-well chamber slides (Thermo Fisher Scientific, Waltham, MA, USA). After seeding (24 h later), spent medium was replaced with fresh medium and the cells were treated with 25 and 100 µg/mL of silica coated IONPs. Cells treated with 5 µM nocodazole were used as positive control. One hour following the treatment the cells were fixed with 4% freshly prepared paraformaldehyde for 10 min, washed with PBS, permeabilized in 0.2% Triton X-100/PBS for 15 min at room temperature and washed with PBS (reagents from Sigma–Aldrich, St. Louis, MO, USA). Before incubation with the primary antibody (overnight at 4 ˚C), the cells were incubated with 7% heat inactivated foetal calf serum + 2% bovine serum albumin in PBS for 30 min at room temperature. Mouse monoclonal anti-β-tubulin (Life Technologies, Grand Island, NY, USA) was used for β-tubulin detection. For the secondary antibody, the affinity pure donkey anti-mouse-TRITC-conjugated antibody was purchased from the Jackson ImmunoResearch Laboratories (West Grove, PA, USA). The secondary antibody was applied to each slide (after their pre-incubation with 5.5% donkey serum in PBS for 30 min at room temperature), incubated for 1 h in the dark and washed (3 × 5 min) with PBS. The nuclei were counterstained with 4′,6-diamidino-2-phenylindole (DAPI) at 1 µg/mL for 1 h. After three washes with PBS, the slides were mounted with an antifading ProLong® Gold mounting medium (Life Technologies, Grand Island, NY, USA). Images of all of the examined slides were obtained by a Nikon epi-fluorescence microscope system Eclipse 80i; the exposure time and dynamic range of the camera in all of the channels were adjusted to the same values for all of the slides to portray quantitatively comparable images. Images were further processed and merged using NIS-Elements Advanced Research 4.13 (instrument and software from Nikon, Tokyo, Japan)

2.11. Cell cycle distribution analysis

HK-2 cells were seeded at a density of 1 500,000 cells/75 cm^2 area tissue culture flasks (Thermo Fisher Scientific, Waltham, MA, USA). After 24 h, the spent medium was replaced with a fresh medium and the cells were treated with 25 and 100 µg/mL of silica coated IONPs for 24 h. Cells treated with 5 µM nocodazole were used as a positive

control. To determine cell cycle distribution, cells were collected, washed with ice-cold PBS, fixed with 70% ethanol and stored at 4 °C for at least 24 h. Next, the cells were pelleted by centrifugation and washed twice with PBS. After subsequent centrifugation, the supernatant was removed and the cells were incubated for 5 min at room temperature in a citrate-phosphate buffer (0.192 M Na_2HPO_4 and 4 mM citric acid, pH 7.8) and then labelled with propidium iodide in Vindelov's solution for 1 h at 37 °C to detect low molecular-weight fragments of DNA [28]. The DNA content was determined using a Dako CyAn flow cytometer (Beckman Coulter, Miami, FL, USA); the excitation wave length was set at 488 nm, the total emission above 560 nm was recorded in FL-3 channel (613/20 nm filter). The data were analysed using Multicycle AV software (Phoenix Flow Systems, San Diego, CA, USA).

2.12. Western blot analysis of p-p53 serine 15 protein level

HK-2 cells were lysed by a cell lysis buffer (Cell Signaling Technology, MA, USA) in line with the manufacturer's instructions after 24 h of treatment with 25 and 100 μg/mL of silica coated IONPs. Cells treated with 500 nM doxorubicin were used as a positive control. The total protein concentration was measured using a Micro-BCA™ Protein Assay Kit (Thermo Fisher Scientific, IL, USA). Purified proteins from treated cells in the amount of 20 μg were loaded onto and run on a polyacrylamide gel. Separated proteins were transferred onto a PVDF membrane (Bio-Rad, CA, USA) in Towbin's system. The membranes were blocked for 1 h with 5% non-fat dry milk in PBST (phosphate buffer saline with 0.05% Tween-20) to prevent non-specific binding. After blocking, the membranes were incubated overnight with a primary antibody against an appropriate antigen (p-p53 serine 15 – Santa Cruz Biotechnology, TX, USA; β-tubulin – Thermo Fisher Scientific, IL, USA) at 4 °C. After incubation, the membranes were washed 4-times with PBST and then incubated with an appropriate secondary antibody (goat anti-rabbit IgG, HRP conjugate – Sigma-Aldrich, MO, USA and goat anti-mouse IgG, HRP conjugate - Thermo Fisher Scientific, IL, USA) for 2 h at room temperature. Finally, the membranes were washed 6-times with PBST and then the bands were detected using a chemiluminescent detection kit (Clarity™ Western ECL Substrate, Bio-Rad, CA, USA). Equal protein loading was verified by reprobing the membranes with an antibody against β-tubulin.

2.13. Analysis of apoptosis

Apoptosis was determined by a CellEvent™ Caspase-3/7 green detection reagent (Life Technologies, Grand Island, NY, USA). Briefly, cells were seeded at a density of 300,000 cells/chamber in 2-well glass chamber slides (Thermo Fisher Scientific, Waltham, MA, USA) and were treated for 24 h with silica coated IONPs 100 μg/mL. HK-2 cells treated with 100 μM cisplatin were used as a positive control. After treatment, the cells were labelled with 5 μL of a CellEvent™ Caspase-3/7 green detection reagent in a complete medium and incubated for 30 min in a humidified 37 °C, CO_2 incubator (5%) in the dark. Images of all of the examined slides were obtained by a Nikon epi-fluorescence microscope system Eclipse 80i; the exposure time and dynamic range of the camera in all of the channels were adjusted to the same values for all of the slides to portray quantitatively comparable images. Images were further processed and merged using NIS-Elements Advanced Research 4.13 (instruments and software from Nikon, Tokyo, Japan).

2.14. Visualization of silica coated IONPs in HK-2 cells

HK-2 cells were seeded at a density of 300,000 cells/chamber in 2-well glass chamber slides (Thermo Fisher Scientific, Waltham, MA, USA). After 24 h of plating, the spent medium was replaced with a fresh medium and the cells were treated with 25 μg/mL and 100 μg/mL of silica coated IONPs. Following 1 h and 24 h of treatment, the cells were washed 3 times with PBS, fixed with a 4% paraformaldehyde/PBS solution and glass coverslips were mounted with a ProLong Gold Antifade Mountant (Life Technologies, Grand Island, NY, USA). The intracellular accumulation of nanoparticles was detected by phase-contrast microscopy using a Nikon Eclipse 80i microscope (Nikon, Tokyo, Japan).

2.15. Statistics

The descriptive statistics of the results were calculated, and the charts were made in Microsoft Office Excel 2010 (Microsoft, Redmond, WA, USA) or GraphPad Prism 6 biostatistics (GraphPad Software, La Jolla, CA, USA). In this study, all the quantitative data were expressed as the arithmetic means with S.D. of triplicates. Statistical significance was analysed after normality testing using one-way analysis of variance (ANOVA), followed by Dunnett's post hoc test. In comparing results with non-treated control cells, the significance level was set at $p = 0.05$.

3. Results

3.1. Preparation and characterization of silica coated IONPs

The hydrophilic nanoparticles of Fe_3O_4 (114 ± 59 nm, DLS) [22] were coated with a layer of amorphous SiO_2, which provided the $Fe_3O4@SiO_2$ IONPs [23]. The reaction of these particles with 3-aminopropyltriethoxysilane resulted in $Fe_3O_4@SiO_2$-NH_2 IONPs with amino groups on the surface [23]. The average size of the Fe3O4@SiO2 IONPs (188 ± 36 nm) and the Fe3O4@SiO2-NH2 IONPs (199 ± 20 nm) [24] was determined by DLS in a phosphate buffer with a pH of 7.3. Further, hydrodynamic particle sizes, PDI and zeta potential were measured in complete cell culture medium in order to investigate size and surface chemistry in relevant experimental condition. The average hydrodynamic size of $Fe_3O_4@SiO_2$ IONPs was 6451 ± 205 nm and PDI was 0.647 ± 0.119. The average hydrodynamic size of $Fe_3O_4@SiO_2$-NH_2 IONPs was 3063 ± 520 nm and PDI was 0.845 ± 0.186. The measurement of the zeta potential of these samples showed -6.52 and -9.77 for $Fe_3O_4@SiO_2$ IONPs and $Fe_3O_4@SiO_2$-NH_2 IONPs, respectively. The specific surface area was found to be 67 m^2/g and 58 m^2/g for $Fe_3O_4@SiO_2$ IONPs and $Fe_3O_4@SiO_2$-NH_2 IONPs, respectively [24].

3.2. The effect of silica coated IONPs on cell proliferation and viability as determined by real-time cellular analysis and XTT assay

The cytotoxic effects of silica coated IONPs against human renal proximal tubular epithelial HK-2 cells were first studied under the standard colorimetric method which measured tetrazolium salt reduction via mitochondrial dehydrogenase activity. Both NH_2-group unfunctionalized and functionalizednanoparticles reduced cell viability in dose dependent manners within 24 h of treatment (Fig. 1A). The antiproliferative effects of silica coated IONPs were further investigated using an xCELLigence system. The xCELLigence system monitors cellular responses in real-time, without exogenous labels by measuring electrical impedance. Microelectrodes integrated in the bottom of special E-Plates provided quantitative information about the biological status of the cells, including cell number, cell adhesion, cell viability and cell morphology. Impedance measurements are displayed as normalized cell index (CI) values, which are directly proportional to cell number. As shown in Fig. 1B, the application of silica coated IONPs at 25 μg/mL decreased the proliferation rate of HK-2 cells compared to 5% PBS vehicle-treated control. Exposure to silica coated IONPs at 50 μg/mL resulted in the almost complete inhibition of cell proliferation with a permanently decreased cell index and no signs of recovery. In contrast, real-time monitoring demonstrated an immediate drop in the cell index in 5% DMSO-treated (positive control) cells. Similarly, but with lower dynamics, application of IONPs at 100, 200 and 400 μg/mL

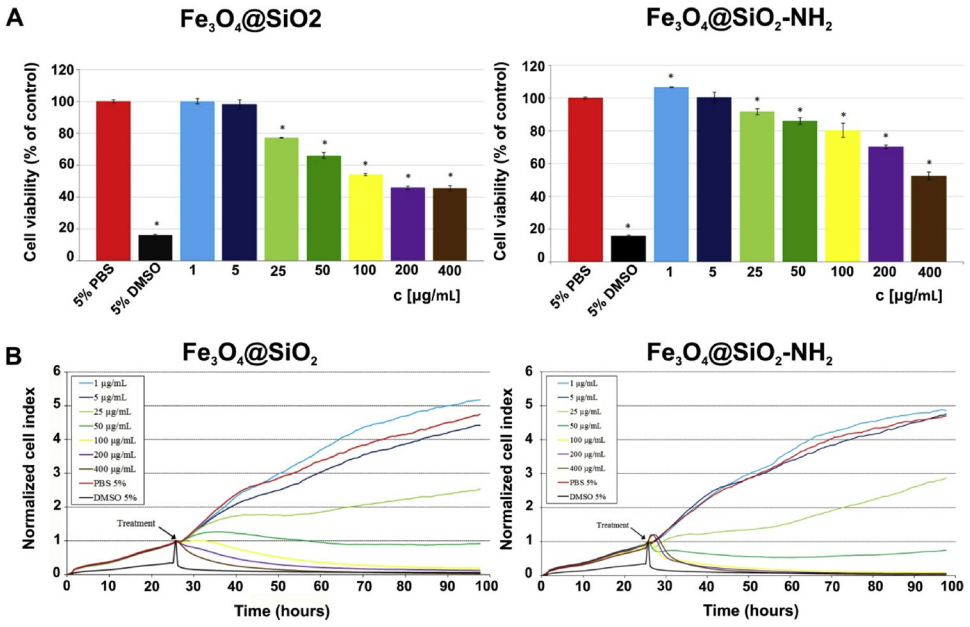

Fig. 1. The effect of silica coated IONPs on the viability and proliferation of HK-2 cells. (A) Cell viability of HK-2 cells measured by using XTT assay 24 h after treatment. Viability is associated with cells treated with 5% PBS (vehicle treatment). Data are shown as mean values ± SD of at least three independent experiments. *Significantly different to control ($P < 0.05$). (B) Dynamic real-time monitoring of cell adhesion, proliferation and cytotoxicity using the xCELLigence system. Cells treated with 5% PBS (vehicle treatment) were used as a negative control while cells treated with 5% DMSO were used as a positive control. The normalized cell index was measured over 72 h.

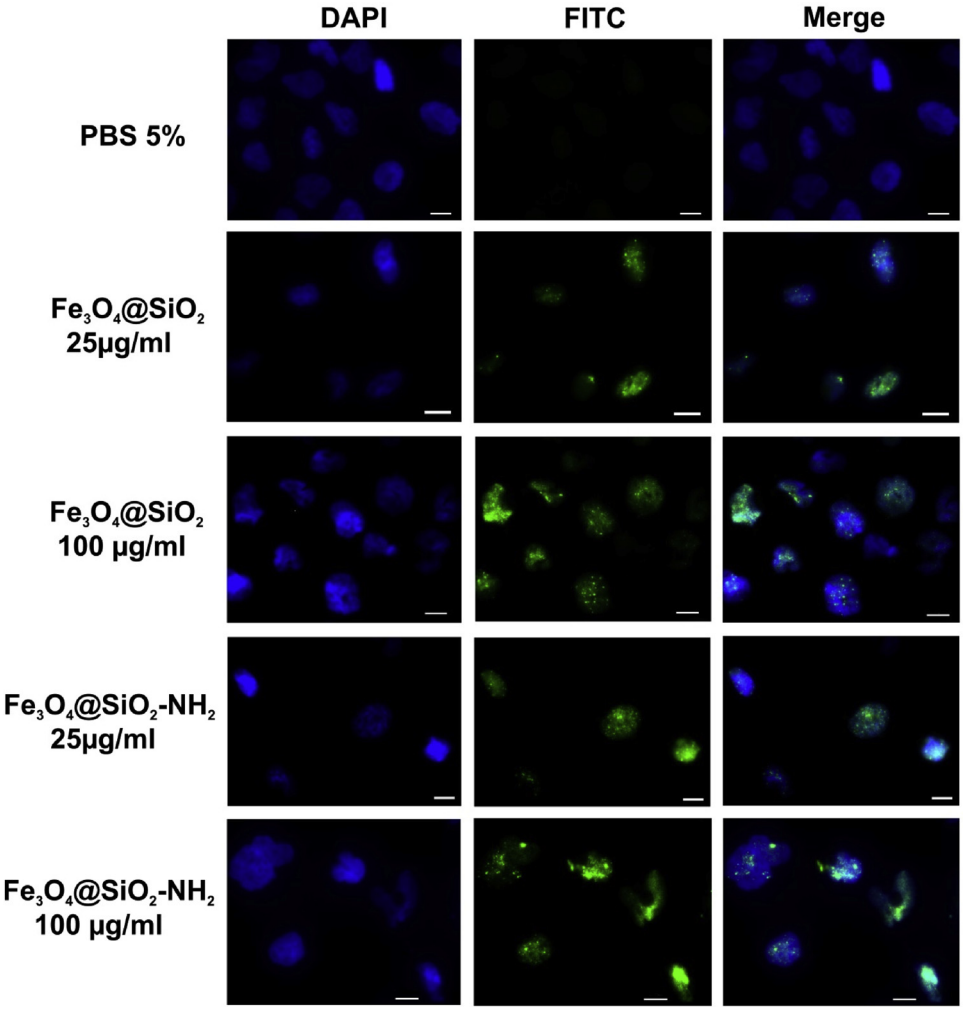

Fig. 2. Microscopic images of HK-2 cells stained with an anti-γH2AX antibody (green) and counterstained with DAPI (blue). The cells were treated with silica coated IONPs or a PBS as a vehicle control. Experiments were performed in triplicate using epi-fluorescence microscopy. Photographs are representative pictures from three independent experiments. The scale bar in the images represents 10 µm.

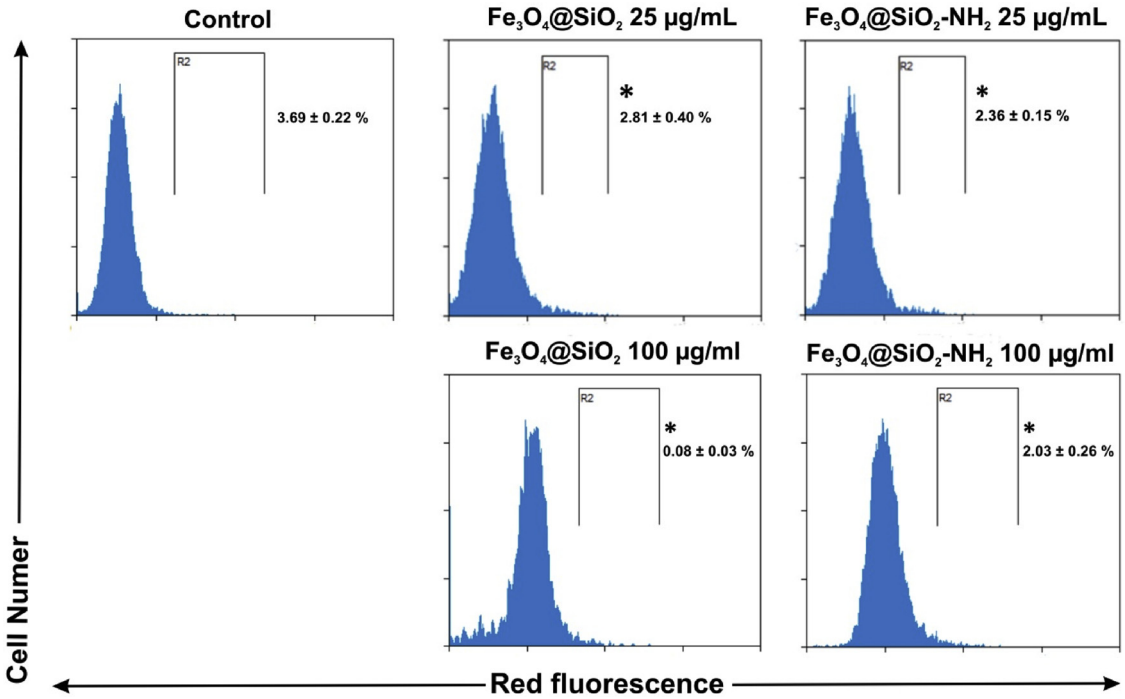

Fig. 3. Production of ROS by silica coated IONPs in HK-2 cells determined by staining with a DHE (dihydroethidium) probe. Cells were treated with silica coated IONPs or a PBS as a vehicle control. Flow cytometry quantitative data are presented as histograms which show the mean percentages of 2-dihydroxyethidium positive cells from three independent experiments ± SD. Representative dot plots of one of the three independent measurements are shown. *Significantly different to control ($P < 0.05$).

caused a decrease in the cell index and cell death.

This set of data, coupled with the results of XTT assay and xCELLigence system, demonstrated that the concentration of 25 µg/mL and above of both determined nanoparticles is cytotoxic, in a known dose-dependent manner. Therefore, to explain the mechanisms of silica coated IONPs cytotoxicity, we decided to investigate concentration 25 µg/mL as sub-cytotoxic and concentration 100 µg/mL as lethal for subsequent tests to avoid unspecific effects caused by significantly decreased cell viability.

3.3. Genotoxicity of silica coated IONPs

The nucleosomal histone protein H2AX is specifically phosphorylated at serine 139 (γH2AX) in response to DNA double-strand breaks (DSBs). Staining for γH2AX accumulated at the DSB-flanking chromatin (foci) is used as a specific marker of DSBs after the action of different genotoxic stresses, including ionizing radiation, environmental agents and chemotherapy drugs [29]. In order to investigate whether silica coated IONPs may cause lethal DNA lesions in the form of DSBs, HK-2 cells were exposed to the nanoparticles for 1 h. As shown in Fig. 2, no obvious γH2AX fluorescent foci were found in the cell nuclei of 5% PBS-treated cells. By contrast, 1 h exposure to 25 and 100 µg/mL of silica coated IONPs substantially increased γH2AX nuclear foci formation in HK-2 cells compared to the negative control (5% PBS). The density and pattern of accumulated γH2AX foci were the same for both types of nanoparticles. Doxorubicin-treated cells were used as a positive control (data not shown), and they exhibited increased γH2AX foci over negative control cells and a more diffuse staining pattern compared to nanoparticle-treated cells.

3.4. The effect of silica coated IONPs on ROS production

Generation of ROS may be one of the mechanisms responsible for the cytotoxicity of nanoparticles. Thus, we assessed the ability of silica coated IONPs to produce ROS. DHE, a specific fluorescent probe for superoxide (O_2^-), was used to track ROS generation in HK-2 cells. H_2O_2 was used as a positive control. The flow cytometric quantification of DHE positive cells revealed no considerable increase in ROS production after treatment with silica coated IONPs for 1 h. Unexpectedly, treatment with silica coated IONPs decreased ROS production (Fig. 3). Treatment of HK-2 cells with H_2O_2 induced significant production of superoxide (data not shown).

3.5. The effect of silica coated IONPs on microtubule cytoskeleton

Cytoskeleton microtubules are involved in the maintenance of cell shape, intracellular trafficking and mitosis. The effect of silica coated IONPs at 25 and 100 µg/mL on the cytoskeletal structure was visually inspected by observing the immunostained cytoskeletal component β-tubulin 1 h after exposure. Epi-fluorescence imaging revealed that mock-treated HK-2 cells had intact microtubules (Fig. 4A). Contrary thereto, treatment with Fe_3O_4@SiO_2-NH_2 IONPs at both examined concentrations of 25 and 100 µg/mL and Fe_3O_4@SiO_2 IONPs at 25 µg/mL resulted in morphological changes, decreased cell body size and a collapsed microtubule network around the cell nuclei (Fig. 4B, D, E). Moreover, treatment with 100 µg/mL Fe_3O_4@SiO_2 IONPs completely disintegrated the microtubule network with weak and diffuse β-tubulin staining dispersed throughout the cytoplasm (Fig. 4C).

3.6. The effect of silica coated IONPs on the distribution of cells in cell cycle phases and analysis of the p53 expression

To better understand the antiproliferative effects of silica coated IONPs, we treated HK-2 cells with 25 and 100 µg/mL of nanoparticles for 24 h and we quantified the percentage of cells in different phases of the cell cycle using flow cytometry. Fe_3O_4@SiO_2 nanoparticles treatment, at 25 µg/mL, resulted in a significant increase in the number of cells in the G1 (77%; control 71%) phase. In contrast, treatment of HK-2 cells with 100 µg/mL Fe_3O_4@SiO_2 nanoparticles resulted in a significant decrease in the number of cells in the G1 (67%; control 71%)

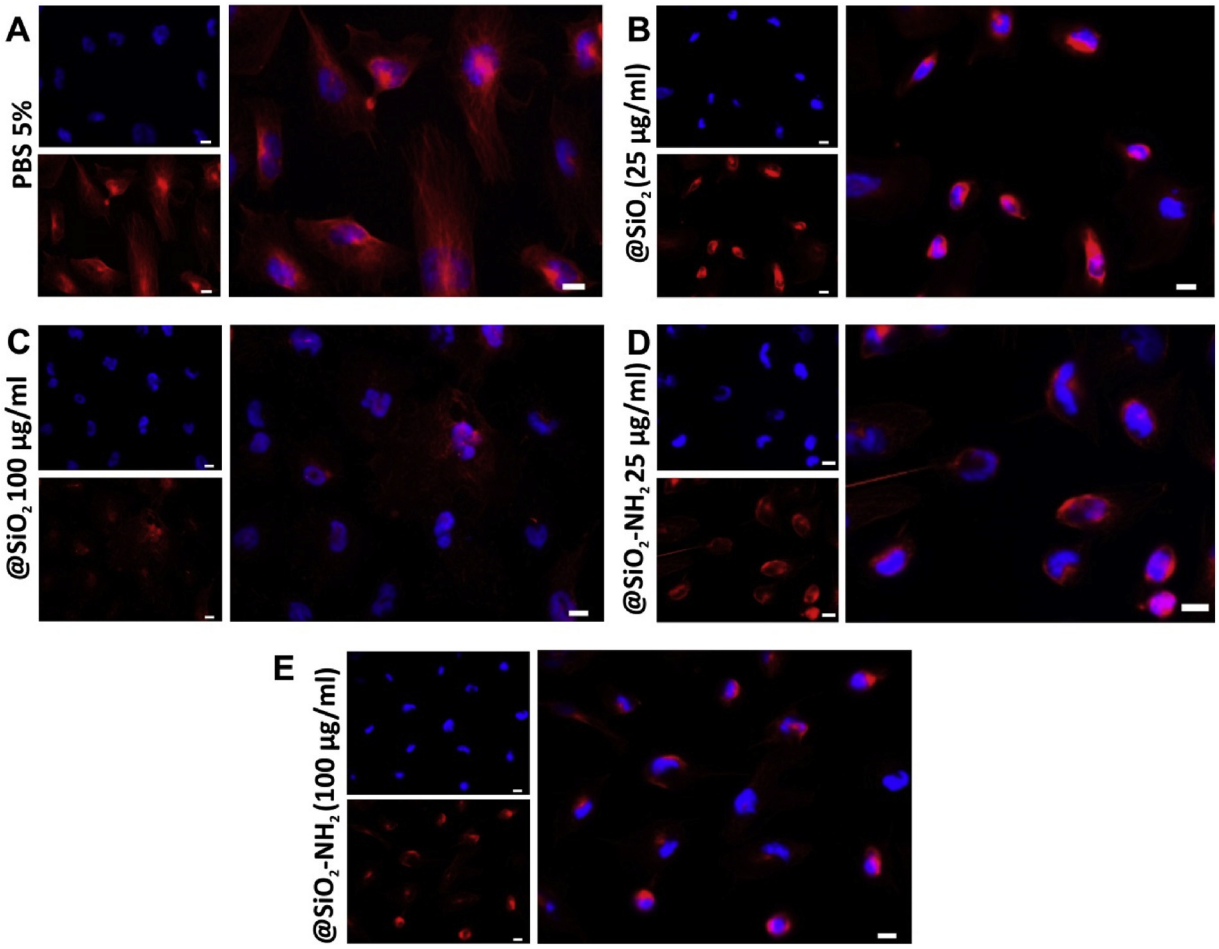

Fig. 4. Microscopic images of HK-2 cells stained with an anti-β-tubulin antibody (red) and counterstained with DAPI (blue). The cells were incubated with PBS (A) or treated with Fe_3O_4@SiO_2 IONPs at 25 (B) and 100 µg/mL (C) or with Fe_3O_4@SiO_2-NH_2 IONPs at 25 (D) and 100 µg/mL (E). Experiments were performed in triplicate using epi-fluorescence microscopy. Photographs from representative chambers are shown. The scale bar in the images represents 10 µm.

phase and a significant increase in the number of cells in the G2/M (22%; control 13%) phase. These effects were concurrently accompanied by a significant decrease in S phase cells (10% for 25 µg/mL, 11% for 100 µg/mL; control 16%) (Fig. 5A). Fe_3O_4@SiO_2-NH_2 IONPs in concentrations of 25 µg/mL and 100 µg/mL induced an increase in the percentage of cells in the G1 (79% and 73%; control 71%) phase and in a concentration of 100 µg/mL also in the G2/M (15%; control 13%) phase of the cell cycle. Exposures to Fe_3O_4@SiO_2-NH_2 IONPs using both examined concentrations were accompanied by a decrease in S phase cells (9% for 25 µg/mL, 11% for 100 µg/mL; control 16%) (Fig. 5B). No sub-G1 peak representing apoptotic cells was seen in the flow cytometry histograms.

As we observed cell cycle delay at 25 and 100 µM, we decided to evaluate the expression of p53 phosphorylated at Ser15 using Western blotting. As shown in Fig. 5C, the exposure of HK-2 cells to silica coated IONPs for 24 h did not result in an increased accumulation of p53 protein phosphorylated at Ser 15.

3.7. Detection of apoptosis

XTT assay and xCELLigence-based measurements revealed that IONPs at 100 µg/mL had a clear negative impact on cell viability, which may be caused by apoptosis - mediated cell death. Apoptosis requires the activation of downstream signalling pathways to orchestrate the activation of caspases. In line with the XTT and xCELLigence-based results of cytotoxicity, we investigated the activation of caspase-3/7 as a hallmark of cell death mediated by apoptosis. As shown in Fig. 6, this characteristic feature of apoptosis was not found after the treatment of HK-2 cells with 100 µg/mL silica coated IONPs for 24 h.

3.8. Visualization of silica coated IONPs

Finally, we traced the subcellular location and distribution of silica coated IONPs to evaluate its direct interaction with the cells. Cells were treated with 100 µg/mL of silica coated IONPs for 1 h and 24 h and cellular accumulation was followed by phase contrast microscopy. Microscopic observations revealed that both types of nanoparticles were internalized into the cytoplasm of HK-2 cells already after 1 h of treatment. The microscopy results regarding the cellular location of silica coated IONPs after a short period of treatment (1 h) displayed the accumulation of silica coated IONPs mainly around the cell membrane. During longer incubation times of 24 h, silica coated IONPs were mainly accumulated in the perinuclear region of the HK-2 cells (Fig. 7).

4. Discussion

It is well known that nanoparticles can spread to various organ systems such as the lungs, brain, heart, spleen, liver, testis, thymus and kidneys [30,31]. The kidneys play a significant role in eliminating myriad toxicants from the body and urinary excretion can be one of the possible routes for eliminating IONPs [32,33]. Theoretically, glomerular filtration, tubular secretion and tubular reabsorption can be involved in the elimination process of nanoparticles. Moreover, nanoparticles with protein corona dispersed in blood plasma reaching the

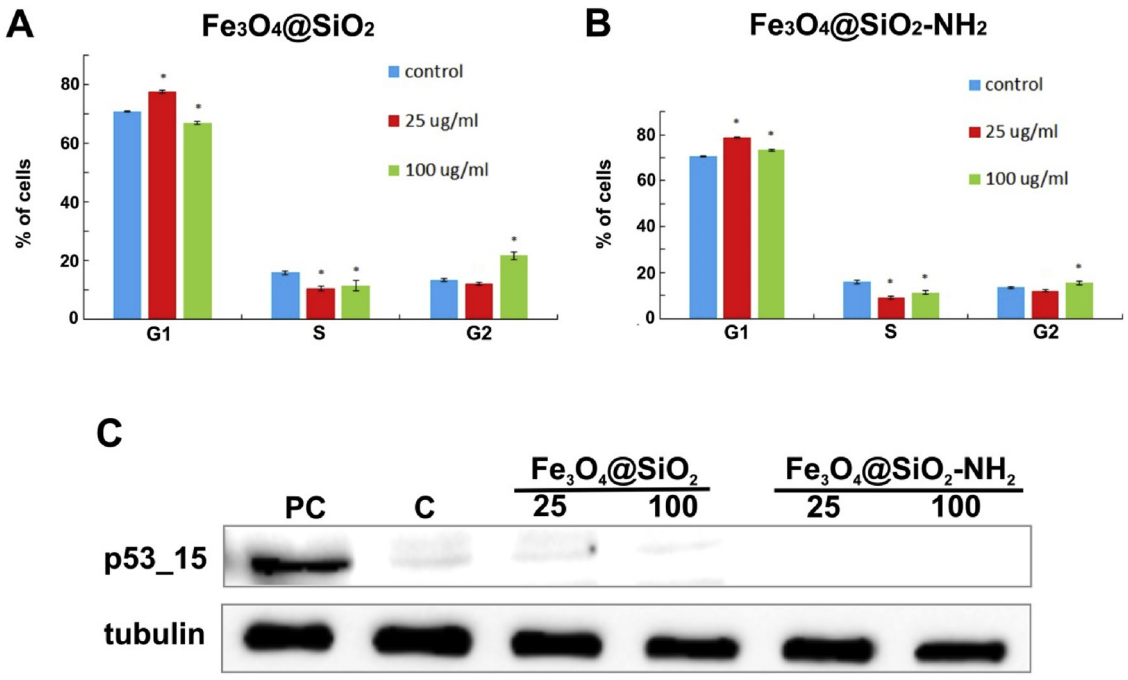

Fig. 5. Analysis of the cell cycle of HK-2 cells 24 h after the application of Fe_3O_4@SiO_2 IONPs (A) and Fe_3O_4@SiO_2-NH_2 IONPs (B) NPs. The bar graph represents the percentage of cells in the G1, S, and G2/M phase of the cell cycle (mean ± SD, n = 3). *Significantly different to control ($P < 0.05$). (C) Western blot analysis of phosphorylated p53 24 h after treatment (p53_15). Cells treated with 500 nM doxorubicin were used as a positive control. These experiments were performed at least three times with similar results and a cropped blot is shown from one representative experiment.

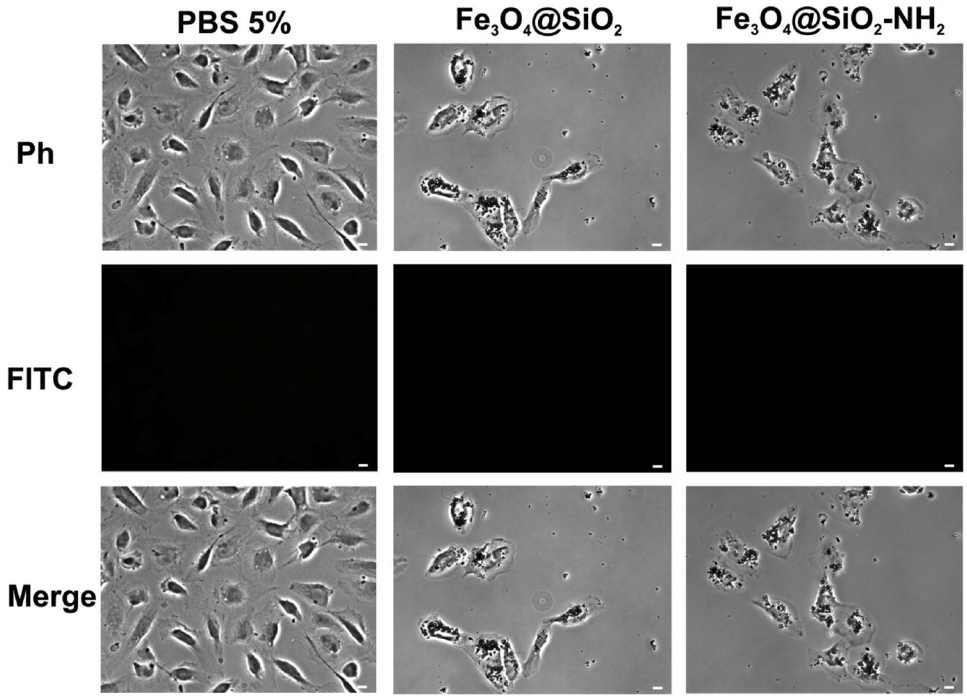

Fig. 6. Microscopy images of the activation of caspase-3/7 in HK-2 cells. The cells were exposed to 100 µg/mL of silica coated IONPs for 24 h. The images showed apoptotic signals of a CellEvent™ Caspase-3/7 Green Detection Reagent (apoptotic cells, green, FITC), corresponding optical phase-contrast microscopy (Ph) and merged images (Merge). Cells treated with 5% PBS (vehicle treatment) were used as a negative control. Photographs are representative pictures from three independent experiments. The scale bar in the images represents 10 µm.

glomerulus but not filtered could potentially damage kidney function. Since the proximal tubule is part of the duct system of the nephron in which the filtrate from the glomerulus enter, and it is a major site for reabsorption and some secretion, we evaluated the *in vitro* antiproliferative and cytotoxic potential of silica coated IONPs on human renal proximal tubule epithelial cells (HK-2) and the mechanism involved in it. We used HK-2 human renal proximal tubule epithelial cells as a model for this study. They have been shown to retain the functional characteristics of the normal human renal proximal tubular cell [34].

First, we assessed the possible cytotoxicity of silica coated IONPs by using an XTT assay. The XTT assay is a standard colorimetric method measuring tetrazolium salt reduction to formazan dye via mitochondrial dehydrogenase activity, which is directly proportional to the number of living cells. Both analysed nanoparticles were found to be cytotoxic at a concentration of 25 µg/mL and above, in a classic dose-dependent manner. Similar results were obtained using the xCELLigence system which enables to get real-time, label-free and non-invasive measurements of cytotoxicity via determining cell

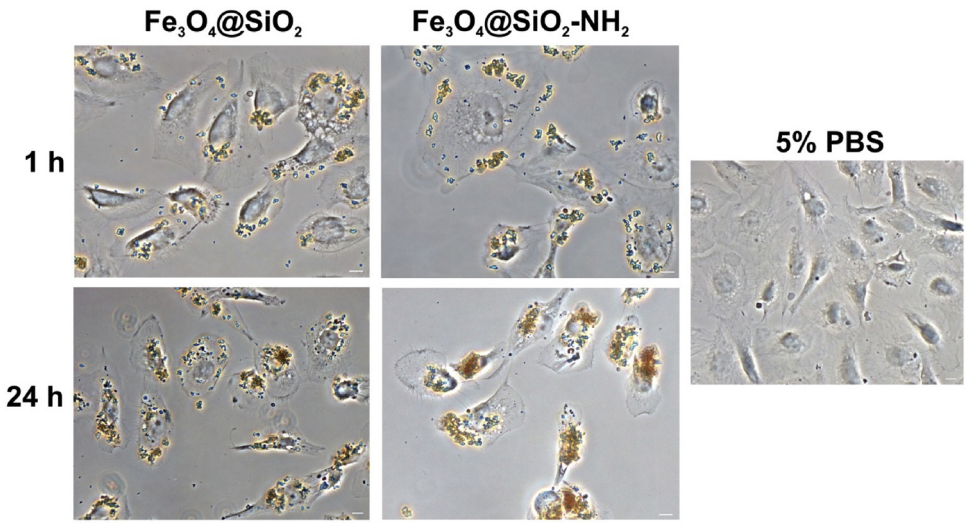

Fig. 7. Accumulation of silica coated IONPs in HK-2 cells. The cells were incubated with 100 µg/mL of silica coated IONPs for 1 h and 24 h and visualized by optical phase-contrast microscopy. Photographs are representative pictures from three independent experiments. The scale bar in the images represents 10 µm.

proliferation as well as cellular survival. This cytotoxic effect of Fe_3O_4@SiO_2 and Fe_3O_4@SiO_2-NH_2 may be related to the fast uptake and accumulation of nanoparticles into cells. Phase-contrast images showed that nanoparticles were accumulated in the cytoplasm of HK-2 cells already 1 h after treatment. Contrary to this, numerous published studies reported no significant cytotoxicity and good biocompatibility following the testing of the biological effects of silica coated IONPs [35,36].

To evaluate the possible genotoxic effects of silica coated IONPs, we performed immunostaining for γH2AX foci as a marker of the most deleterious DNA damage, the DNA double-strand breaks. Our results show that short-term exposure (1 h) of the HK-2 cells to both the investigated types of silica coated IONPs at two different concentrations, namely 25 and 100 µg/mL, resulted in severe DNA damage, i.e. lethal DNA lesions in the form of DSBs. Also, some studies have reported that silica coated IONPs can induce cytotoxicity and DNA damage in L5178Y cells [37], A549 and HeLa cells [38] which is similar to our findings using HK-2 human renal proximal tubule epithelial cells as a model.

Generation of ROS represents one of the most dominant mechanisms responsible for the toxicity and genotoxicity of nanoparticles [39–41]. Thus, we assessed the ability of silica coated IONPs to induce the production of intracellular oxidants in HK-2 cells, using DHE as a fluorescent probe for the detection of ROS generation. Surprisingly, our data showed no increased intracellular ROS generation following exposure to both analysed silica coated IONPs. This result is contradictory to findings stated in the study published by Malvindi and colleagues in which bare (Fe_3O_4@SiO_2) nanoparticles were found to produce a significant increase in ROS levels. Similarly, passivated (Fe_3O_4@SiO_2-NH_2) nanoparticles stimulate prooxidant reactions, however, they induce the generation of low levels of ROS [38]. Recently, some authors showed that IONPs can affect cytoskeletal proteins, which subsequently leads to the disruption of cell homeostasis and physiological cellular processes [42,43]. Therefore, we investigated the effect of silica coated IONPs on the microtubule cytoskeleton. Our results demonstrated that silica coated IONPs abolish the formation of long and extended microtubules. This resulted in the microtubule network breaking up into individual microtubules focused around the cell nuclei in dense bundles. Furthermore, treatment with 100 µg/mL Fe_3O_4@SiO_2 nanoparticles completely disintegrated the microtubule network. These results corresponded with other studies that found significant cytoskeleton changes after IONPs exposure. Soenen et al. reported that both the actin cytoskeleton and microtubule network undergo a significant remodelling when human blood outgrowth endothelial cells are incubated with Resovist (carboxydextran-coated IONPs) or magnetoliposomes. Endorem (dextran-coated IONPs) particles also influence the cytoskeletal networks at higher concentrations [43]. Highly apparent cytoskeleton disruption, disorganization of actin fibres and tubulin networks were observed in human umbilical vein endothelial cells treated with citric acid and dextran coated IONPs [42]. In consistence with these reports, Mesárošová et al. and co-workers found visible changes in HEL 12469 human embryonic lung fibroblast cell morphology following exposure to surface-modified magnetite nanoparticles. The authors speculated that not only internalized amount of magnetite nanoparticles, but also inter-action of magnetite nanoparticles with the cytoskeletal proteins can lead to disruption of cell homeostasis or other fundamental cellular physiological processes [44].

To further elucidate the mechanism of antiproliferative activity and cytotoxicity of silica coated IONPs, we analysed cell cycle phase distribution, activation of caspase-*3/7* as a hallmark of apoptosis, and expression of p53 and its Ser15 phosphorylated form. The results of cell cycle distribution evaluated through flow cytometric analysis demonstrated that both silica coated IONPs were able to affect the cell cycle distribution of HK-2 cells. We found that treatment with silica coated IONPs preferably induced the cell cycle accumulation of HK-2 cells at the G1 phase at low concentration and G2/M phases phase at higher concentration. The previous study on human hepatoma BEL-7402 cells showed that Fe_3O_4 and oleic acid-coated Fe_3O_4 induced G1 cell cycle arrest [45]. In contrast to this, the treatment of BEL-7402 cells with carbon-coated Fe nanoparticles caused G2/M cell cycle arrest [45]. Therefore, we can assume that the Fe_3O_4@SiO_2 and Fe_3O_4@SiO_2-NH_2 nanoparticles mechanism regarding cell cycle progression might be different to that reported for Fe_3O_4, OA-Fe_3O_4 and carbon-coated Fe nanoparticles.

Since the activation of caspase-3-like proteases, such as caspase-3 and caspase-7, is one of the markers observed during apoptosis, we examined the activation of caspase 3/7 using fluorescence microscopy and a fluorogenic substrate for activated caspase-3/7. However, using the above-mentioned technique, this characteristic feature of apoptosis was not found after the exposure of HK-2 cells to 100 µg/mL of silica coated IONPs. p53 is a well-established tumour suppressor protein that plays a key role in cell cycle regulation and in cellular response to genotoxic and cytotoxic stress [46]. In response to various stress signals such as DNA damage, the p53 protein is activated by posttranslational modifications and the follow-up induction of various p53 target genes leads to cell cycle arrest, apoptosis or cell senescence [47,48]. In this study, the expression level of phospho-p53 (Ser15) was analysed by

Western blot analysis. Surprisingly, treatment with silica coated IONPs did not result in an increased level of p53 protein phosphorylated at serine 15.

These observations indicate that the p53 signalling pathways were not affected by treatment with silica coated IONPs. These findings are inconsistent with those of Ng et al. who demonstrated that ZnO nanoparticles are capable of causing DNA double-strand break (DSBs) signalling in mammalian cells. Most significantly, Ng et al. showed that the genotoxic influence of ZnO nanoparticles resulted in the activation of p53 [49].

5. Conclusions

We may conclude that silica coated IONPs had antiproliferative, cytotoxic and genotoxic effects on HK-2 human renal proximal tubule epithelial cells. Silica coated IONPs induced severe disruption of the microtubule cytoskeleton structure, decreasing the cell proliferation rate, and led to DNA double-strand breaks. Highly damaged HK-2 cells might be lost via necrosis as none of the two analysed silica coated IONPs induced apoptosis or increased accumulation of phospho-p53 (Ser15).

Conflict of interest

None.

Acknowledgments

We wish to thank Ivana Fousová for her skilful technical assistance. This study was financially supported by Grant Project No. 18-13323S of the Czech Science Foundation.

References

[1] Y. Wang, C. Xu, H. Ow, Commercial Nanoparticles for Stem cell labeling and tracking, Theranostics 3 (2013) 544–560, https://doi.org/10.7150/thno.5634.
[2] C. Wilhelm, F. Gazeau, Universal cell labelling with anionic magnetic nanoparticles, Biomaterials 29 (2008) 3161–3174, https://doi.org/10.1016/j.biomaterials.2008.04.016.
[3] D. Lago-Cachón, M. Rivas, C. López-Larrea, A. López-Vázquez, G. Martínez-Paredes, J.A. García, HeLa cells separation using MICA antibody conjugated to magnetite nanoparticles, Phys. Status. Solidi C 11 (2014) 1043–1047, https://doi.org/10.1002/pssc.201300729.
[4] M.A. Malvindi, A. Greco, F. Conversano, A. Figuerola, M. Corti, M. Bonora, A. Lascialfari, H.A. Doumari, M. Moscardini, R. Cingolani, G. Gigli, S. Casciaro, T. Pellegrino, A. Ragusa, Magnetic/Silica nanocomposites as dual-mode contrast agents for combined magnetic resonance imaging and ultrasonography, Adv. Funct. Mater. 21 (2011) 2548–2555, https://doi.org/10.1002/adfm.201100031.
[5] P. Yi, G. Chen, H. Zhang, F. Tian, B. Tana, J. Dai, Q. Wang, Z. Deng, Magnetic resonance imaging of Fe3O4@SiO2-labeled human mesenchymal stem cells in mice at 11.7 T, Biomaterials 34 (2013) 3010–3019, https://doi.org/10.1016/j.biomaterials.2013.01.022.
[6] F. Gazeau, M. Levy, C. Wilhelm, Optimizing magnetic nanoparticle design for nanothermotherapy, Nanomedicine 3 (2008) 831–844, https://doi.org/10.2217/17435889.3.6.831.
[7] J. Klostergaard, C.E. Seeney, Magnetic nanovectors for drug delivery, Nanomedicine 8 (2012) S37–50, https://doi.org/10.1016/j.nano.2012.05.010.
[8] M. Sedlák, D.S. Bhosale, L. Beneš, J. Palarčík, A. Kalendová, K. Královec, A. Imramovský, Synthesis and characterization of a pH-sensitive conjugate of isoniazid with Fe3O4@SiO2 magnetic nanoparticles, Bioorg. Med. Chem. Lett. 23 (2013) 4692–4695, https://doi.org/10.1016/j.bmcl.2013.05.103.
[9] K. Rudzka, J.L. Viota, J.A. Muñoz-Gamez, A. Carazo, A. Ruiz-Extremera, Á.V. Delgado, Nanoengineering of doxorubicin delivery systems with functionalized maghemite nanoparticles, Colloids Surf, B. Biointerfaces 111 (2013) 88–96, https://doi.org/10.1016/j.colsurfb.2013.05.010.
[10] C. Plank, O. Zelphati, O. Mykhaylyk, Magnetically enhanced nucleic acid delivery. Ten years of magnetofection-progress and prospects, Adv. Drug Deliv. Rev. 63 (2011) 1300–1331, https://doi.org/10.1016/j.addr.2011.08.002.
[11] P. Reimer, T. Balzer, Ferucarbotran (Resovist): a new clinically approved RES-specific contrast agent for contrast-enhanced MRI of the liver—properties, clinical development, and applications, Eur. Radiol. 13 (2003) 1266–1276, https://doi.org/10.1007/s00330-002-1721-7.
[12] W. Pfaller, G. Gstraunthaler, Nephrotoxicity testing in vitro – what we know and what we need to know, Environ. Health Perspect. 106 (1998) 559–569, https://doi.org/10.1289/ehp.98106559.
[13] Z. Chen, H. Meng, G. Xing, C. Chen, Y. Zhao, G. Jia, T. Wang, H. Yuan, C. Ye, F. Zhao, Z. Chai, C. Zhu, X. Fang, B. Ma, L. Wan, Acute toxicological effects of copper nanoparticles in vivo, Toxicol. Lett. 163 (2006) 109–120, https://doi.org/10.1016/j.toxlet.2005.10.003.
[14] J.X. Wang, G. Zhou, C. Chen, H. Yu, T. Wang, Y. Ma, G. Jia, Y. Gao, B. Li, J. Sun, Y. Li, F. Jiao, Y. Zhao, Z. Chai, Acute toxicity and biodistribution of different sized titanium dioxide particles in mice after oral administration, Toxicol. Lett. 168 (2007) 176–185, https://doi.org/10.1016/j.toxlet.2006.12.001.
[15] A. Hanini, A. Schmitt, K. Kacem, F. Chau, S. Ammar, J. Gavard, Evaluation of iron oxide nanoparticle biocompatibility, Int. J. Nanomed. Nanosurg. 6 (2011) 787–794, https://doi.org/10.2147/IJN.S17574.
[16] B. L'Azou, J. Jorly, D. On, E. Sellier, F. Moisan, J. Fluery-Feith, J. Cambar, P. Brochard, Ohayon-Courtes C. In vitro effects of nanoparticles on renal cells, Part. Fibre Toxicol. 5 (2008) 22, https://doi.org/10.1186/1743-8977-5-22.
[17] A. Kermanizadeh, S. Vranic, S. Boland, K. Moreau, A. Baeza-Squiban, B.K. Gaiser, L.A. Andrzejczuk, V. Stone, An in vitro assessment of panel of engineered nanomaterials using a human renal cell line: cytotoxicity, pro-inflammatory response, oxidative stress and genotoxicity, BMC Nephrol. 14 (2013) 96, https://doi.org/10.1186/1471-2369-14-96.
[18] I. Pujalté, I. Passagne, B. Brouillaud, M. Tréguer, E. Durand, C. Ohayon-Courtès, B. L'Azou, Cytotoxicity and oxidative stress induced by different metallic nanoparticles on human kidney cells, Part. Fibre Toxicol. 8 (2011) 10, https://doi.org/10.1186/1743-8977-8-10.
[19] W. Wu, Q. He, C. Jiang, Magnetic iron oxide nanoparticles: synthesis and surface functionalization strategies, nanoscale res, Lett. 3 (2008) 397–415, https://doi.org/10.1007/s11671-008-9174-9.
[20] M.A. Malvindi, V. Brunetti, G. Vecchio, A. Galeone, R. Cingolani, P.P. Pompa, SiO2 nanoparticles biocompatibility and their potential for gene delivery and silencing, Nanoscale 4 (2012) 486–495, https://doi.org/10.1039/c1nr11269d.
[21] G. Bardi, M.A. Malvindi, L. Gherardini, M. Costa, P.P. Pompa, R. Cingolani, T. Pizzorusso, The biocompatibility of amino functionalized CdSe/ZnS quantum dot-doped SiO2 nanoparticles with primary neural cells and their gene carrying performance, Biomaterials 31 (2010) 6555–6566, https://doi.org/10.1016/j.biomaterials.2010.04.063.
[22] C. Hui, C. Shen, T. Yang, L. Bao, J. Tian, H. Ding, C. Li, H. Gao, Large-scale Fe3O4 nanoparticles soluble in water synthesized by a facile method, J. Phys. Chem. C 112 (2008) 11336–11339, https://doi.org/10.1021/jp801632p.
[23] S.A. McCarthy, G. Davies, Y.K. Gun'ko, Preparation of multifunctional nanoparticles and their assemblies, Nat. Protoc. 7 (2012) 1677–1693, https://doi.org/10.1038/nprot.2012.082.
[24] M. Slováková, M. Sedlák, B. Křižíková, R. Kupčík, Bulánek R, L. Korecká, Č. Drašar, Z. Bílková, Application of trypsin Fe_3O_4@SiO_2 core/shell nanoparticles for protein digestion, Process Biochem. 50 (2015) 2088–2098, https://doi.org/10.1016/j.procbio.2015.09.002.
[25] M. Van de Waterbeemd, T. Sen, S. Biagini, I.J. Bruce, Surface functionalisation of magnetic nanoparticles: quantification of surface to bulk amine density, Micro Nano Lett. 5 (2010) 282–285, https://doi.org/10.1049/mnl.2010.0112.
[26] R. Havelek, P. Siman, J. Cmielova, A. Stoklasova, J. Vavrova, J. Vinklarek, J. Knizek, M. Rezacova, Differences in vanadocene dichloride and cisplatin effect on MOLT-4 leukemia and human peripheral blood mononuclear cells, Med. Chem. (Los Angeles) 8 (2012) 615–621, https://doi.org/10.2174/157340612801216364.
[27] H. Zhao, J. Joseph, H.M. Fales, E.A. Sokoloski, R.L. Levine, J. Vasquez-Vivar, B. Kalyanaraman, Detection and characterization of the product of hydroethidine and intracellular superoxide by HPLC and limitations of fluorescence, Proc. Natl. Acad. Sci. U. S. A. 102 (2005) 5727–5732, https://doi.org/10.1073/pnas.0501719102.
[28] Z. Darzynkiewicz, G. Juan, X. Li, W. Gorczyca, T. Murakami, F. Traganos, Cytometry in cell necrobiology: analysis of apoptosis and accidental cell death (necrosis), Cytometry 27 (1997) 1–20, https://doi.org/10.1016/S0037-1963(01)90051-4.
[29] L.J. Kuo, L.X. Yang, γ-H2AX – a novel biomarker for DNA double-strand breaks, In Vivo 22 (2008) 305–309.
[30] W.H. De Jong, W.I. Hagens, P. Krystek, M.C. Burger, A.J. Sips, R.E. Geertsma, Particle size-dependent organ distribution of gold nanoparticles after intravenous administration, Biomaterials 29 (2008) 1912–1919, https://doi.org/10.1016/j.biomaterials.2007.12.037.
[31] T.K. Jain, M.K. Reddy, M.A. Morales, D.L. Leslie-Pelecky, V. Labhasetwar, Biodistribution, clearance, and biocompatibility of iron oxide magnetic nanoparticles in rats, Mol. Pharm. 5 (2008) 316–327, https://doi.org/10.1021/mp7001285.
[32] A.A. Burns, J. Vider, H. Ow, E. Herz, O. Penate-Medina, M. Baumgart, S.M. Larson, U. Wiesner, M. Bradbury, Fluorescent silica nanoparticles with efficient urinary excretion for nanomedicine, Nano Lett. 9 (2009) 442–448, https://doi.org/10.1021/nl803405h.
[33] J. Liu, M. Yu, C. Zhou, J. Zheng, Renal clearable inorganic nanoparticles: a new frontier of bionanotechnology, Mater. Today 16 (2013) 477–486, https://doi.org/10.1016/j.mattod.2013.11.003.
[34] P. Gunness, K. Aleksa, K. Kosuge, S. Ito, G. Koren, Comparison of the novel HK-2 human renal proximal tubular cell line with the standard LLC-PK1 cell line in studying drug-induced nephrotoxicity, Can. J. Physiol. Pharmacol. 88 (2010) 448–555, https://doi.org/10.1139/y10-023.
[35] X. Guo, F. Mao, W. Wang, Y. Yang, Z. Bai, Sulfhydryl-modified Fe3O4@SiO2 core/shell nanocomposite: synthesis and toxicity assessment *in vitro*, ACS Appl. Mater. Interfaces 7 (2015) 14983–14991, https://doi.org/10.1021/acsami.5b03873.
[36] M.Z. Iqbal, X. Ma, T. Chen, L.E. Zhang, W. Ren, L. Xiang, A. Wu, Silica-coatedsuperparamagnetic iron oxide nanoparticles (SPIONPs): a new type contrast agent of *T*1

ARTICLE IN PRESS

magneticresonance imaging (MRI), J. Mater. Chem. B Mater. Biol. Med. 3 (2015) 5172–5181, https://doi.org/10.1039/c5tb00300h.
[37] J.S. Kang, Y.N. Yum, S.N. Park, Cytotoxicity and DNA damage induced by magnetic nanoparticle silica in L5178Y cell, Biomol. Ther. (Seoul) 19 (2011) 261–266, https://doi.org/10.4062/biomolther.2011.19.2.261.
[38] M.A. Malvindi, V. de Matteis, A. Galeone, V. Brunetti, G.C. Anyfantis, A. Athanassiou, R. Cingolani, P.P. Pompa, Toxicity assessment of silica coated iron oxide nanoparticles and biocompatibility improvement by surface engineering, PLoS One 9 (2014) e85835, , https://doi.org/10.1371/journal.pone.0085835.
[39] P.V. Asharani, G. Low Kah Mun, M.P. Hande, S. Valiyaveettil, Cytotoxicity and genotoxicity of sliver nanoparticles in human cells, ACS Nano 3 (2009) 279–290, https://doi.org/10.1021/nn800596w.
[40] H.R. Kim, M.J. Kim, S.Y. Lee, S.M. Oh, K.H. Chung, Genotoxic effects of silver nanoparticles stimulated by oxidative stress in human bronchial epithelial (BEAS-2B) cells, Mutat. Res. Genet. Toxicol. Environ. Mutagen. 726 (2011) 129–135, https://doi.org/10.1016/j.mrgentox.2011.08.008.
[41] N. Singh, G.J. Jenkins, B.C. Nelson, B.J. Marquis, T.G. Maffeis, A.P. Brown, P.M. Williams, C.J. Wright, S.H. Doak, The role of iron redox state in the genotoxicity of ultrafine superparamagnetic iron oxide nanoparticles, Biomaterials 33 (2012) 163–170, https://doi.org/10.1016/j.biomaterials.2011.09.087.
[42] X. Wu, Y. Tan, H. Mao, M. Zhang, Toxic effects of iron oxide nanoparticles onhuman umbilical vein endothelial cells, Int. J. Nanomed. Nanosurg. 5 (2010) 385–399, https://doi.org/10.2147/IJN.S10458.
[43] S.J. Soenen, N. Nuytten, S.F. De Meyer, S.C. De Smedt, M. De Cuyper, High intracellular iron oxide nanoparticle concentrations affect cellular cytoskeleton and focal adhesion kinase-mediated signaling, Small. 6 (2010) 832e42, , https://doi.org/10.1002/smll.200902084.
[44] M. Mesárošová, K. Kozics, A. Bábelová, E. Regendová, M. Pastorek, D. Vnuková, B. Buliaková, F. Rázga, A. Gábelová, The role of reactive oxygen species in the genotoxicity of surface-modified magnetite nanoparticles, Toxicol. Lett. 226 (2014) 303–313, https://doi.org/10.1016/j.toxlet.2014.02.025.
[45] W. Kai, X. Xiaojun, P. Ximing, H. Zhenqing, Z. Qiqing, Cytotoxic effects and the mechanism of three types of magnetic nanoparticles on human hepatoma BEL-7402 cells, Nanoscale Res. Lett. 6 (2011) 480, https://doi.org/10.1186/1556-276X-6-480.
[46] A.J. Levine, p53, the cellular gatekeeper for growth and division, Cell 88 (1997) 323–331, https://doi.org/10.1016/S0092-8674(00)81871-1.
[47] C. Prives, P.A. Hall, The p53 pathway, J. Pathol. 187 (1999) 112–126, https://doi.org/10.1002/(SICI)1096-9896(199901)187:1%3C112::AID-PATH250%3E3.0.CO;2-3.
[48] L.J. Hofseth, S.P. Hussain, C.C. Harris, p53: 25 years after its discovery, Trends Pharmacol, Sci. 25 (2004) 177–181, https://doi.org/10.1016/j.tips.2004.02.009.
[49] K.W. Ng, S.P. Khoo, B.C. Heng, M.I. Setyawati, E.C. Tan, X. Zhao, S. Xiong, W. Fang, D.T. Leong, J.S. Loo, The role of the tumor suppressor p53 pathway in the cellular DNA damage response to zinc oxide nanoparticles, Biomaterials 32 (2011) 8218–8225, https://doi.org/10.1016/j.biomaterials.2011.07.036.